frontiers | Frontiers in Earth Science

TYPE Original Research
PUBLISHED 19 June 2023
DOI 10.3389/feart.2023.1200079

OPEN ACCESS

EDITED BY
Yubing Liu,
China University of Mining and Technology, China

REVIEWED BY
Xiangfeng Guo,
National University of Singapore, Singapore
Zhanping Song,
Xi'an University of Architecture and Technology, China
Chen Dongfang,
Wuhan University of Technology, China
Yan Zhang,
Chengdu University of Technology, China

*CORRESPONDENCE
Haoteng Wang,
Ironhookbrother@gmail.com
Ying Zhao,
Zhaoyin856@126.com

RECEIVED 04 April 2023
ACCEPTED 31 May 2023
PUBLISHED 19 June 2023

CITATION
Xue H, Wang H, Li L, Gong X, Zhao Y, Zhao J and Zhang Y (2023), Influence of stone content on face stability for tunnels in sandy cobble strata.
Front. Earth Sci. 11:1200079.
doi: 10.3389/feart.2023.1200079

Influence of stone content on face stability for tunnels in sandy cobble strata

Haifang Xue[1,2], Haoteng Wang[3]*, Lingyun Li[1,2], Xiaoqin Gong[1,2], Ying Zhao[4]*, Jianbin Zhao[5] and Yonghao Zhang[5]

[1]Qinghai Traffic Investment Co., Ltd., Xining, China, [2]Qinghai Xihu Expressway Management Co., Ltd., Xining, China, [3]State Key Laboratory of Eco-Hydraulics in Northwest Arid Region, Xi'an University of Technology, Xi'an, China, [4]School of Highway, Chang'an University, Xi'an, China, [5]China National Logging Corporation, Xi'an, China

As a result of the complex geological conditions of sand-cobble stratum, various types of problems may arise during construction of tunnels crossing sand-cobble stratum, the most prominent of which is the stability problem of the face. In order to study the stability of the tunnel face in sand-cobble stratum, first, a continuous medium model of sandstone soil is established, and numerical simulation is carried out on the three-axis compression test of sandstone soil to analyze its micro-mechanical characteristics. Second, a calculation model of simulated sandstone strata excavation is established by FLAC3D finite difference software. Then, the safety factor K calculated by the strength reduction method is introduced as the evaluation index of the face stability, and the face stability of sand-cobble tunnels with a series of stone content, tunnel burial depth and tunnel diameter are analyzed. The results show that the macro stress-strain curve of sand-cobble soil in the three-axis compression test can be divided into linear stage, elastic-plastic stage and ideal plastic stage, and the shear strength of sand-cobble soil increases with the increase of stone content. In the process of tunnel excavation, the stability of tunnel face increases with the increase of stone content in the stratum; while the tunnel buried depth and diameter increase, the stability of tunnel face decreases. These results provide a reference for predicting the instability and failure of sand-cobble tunnels, which is critical for the construction and safety of tunnels in sand-cobble stratum.

KEYWORDS

numerical simulation, sandy cobble stratum, stability of tunnel face, stone content, safety factor

1 Introduction

The tunnel of the project traverses a sandy cobble stratum, which represents a distinctive soil-rock mixture consisting of rock blocks with specific dimensions and high strength, combined with low-strength soil. This stratum exhibits geotechnical properties that significantly differ from those encountered in conventional engineering practices. During tunnel excavation, the uneven distribution and substantial dispersion of cobble particles often lead to over-excavation challenges and hinder the formation of a stable tunnel. The roof and sidewalls of the tunnel are prone to deformation, making collapse and roof falls more likely to occur. Without timely and appropriate support, the rock surrounding the tunnel face may become destabilized and collapse, resulting in ground settlement, deformation, and collapse. Hence, the investigation of tunnel face stability in the sandy cobble stratum holds paramount importance in such excavation scenarios.

Numerous scholars have conducted extensive research on the mechanical properties of sand-cobble mixture and the stability of the face during tunnel excavation under geological conditions. Some scholars have used the discrete element method to establish a numerical model of sand-cobble mixture and performed uniaxial loading tests, which showed good consistency between the numerical simulation results and *insitu* tests in terms of nonlinear deformation and failure mode (Wang et al., 2005). In addition, many scholars have studied the shear characteristics of the soil-rock mixture through the discrete element method and found that the shear characteristics of the soil-rock mixture are mainly related to factors such as the stone content and moisture content, with the stone content having a greater impact on the shear characteristics of the soil-rock mixture (Medley and SanzRehermann, 2004; Xu et al., 2014; Kalender et al., 2014; Zhang et al., 2016; Napoli et al., 2018a; Napoli et al., 2018b, 2019; Napoli et al., 2021). Regarding the issue of large deformation caused by tunnel excavation, many scholars have analyzed the stability of the face using analytical, experimental, and numerical simulation methods (Augarde et al., 2003; Chen et al., 2011; Ukritchon and Keawsawasvong, 2017). Due to the good reproducibility of numerical simulation methods, they have been widely applied to the study of instability and failure modes of tunnel faces (Huang et al., 2018; Ukritchon and Keawsawasvong, 2019a; Ukritchon and Keawsawasvong, 2019b, c; Ukritchon et al., 2019). Based on these failure mechanisms, many scholars have conducted extensive research on the factors affecting and improving the stability of the face (Zhang et al., 2015; Han et al., 2016a; Han et al., 2016b; Li and Zhang, 2020). Despite the progress made in the study of face stability, there are still some limitations. Currently, in numerical experiments on the stability of sand-cobble strata tunnel faces, the sand-cobble stratum is usually treated as a homogeneous material. However, sandy cobble stratum is a heterogeneous material with large and random cobble size distribution, and its internal structure characteristics have an important influence on the overall mechanical properties (Zhang et al., 2023). Moreover, the stone content has been proven to be an important factor affecting the mechanical properties of the sand-cobble mixture, but there are relatively few studies on the influence of the stone content on the stability of sand-cobble tunnel faces. Therefore, given the geological conditions of the engineering project, it is necessary to conduct research on the stability of tunnel faces under the influence of stone content.

In numerical simulation methods, the Finite Element Method (FEM) suffers from the drawback of ill-conditioned mesh dependence when analyzing localization problems. In comparison to FEM and Finite Difference Method (FDM), Discrete Element Method (DEM) is highly time-consuming when simulating failure in tunnel surfaces. Furthermore, the microscale parameters inputted into DEM from parameter calibration are challenging to represent the true characteristics of the soil. The three-dimensional Finite Difference code FLAC3D (Itasca Consulting Group, 2006) utilizes an explicit Lagrangian computational scheme and hybrid discretization zoning technique. It is a forward scheme designed for nonlinear problems, eliminating the need for iteration, unlike other techniques such as FEM using implicit solution methods. Additionally, FLAC3D performs well in handling large deformation problems. In this study, tunnel excavation calculations will be modeled using FLAC3D software.

In the field of geotechnical engineering, the strength reduction method is often used to analyze the safety factor of geotechnical soils, and some related scholars have combined the strength reduction method with the finite element or finite difference method (Zhang et al., 2006; Zhang et al., 2007; Zheng et al., 2008; Qiao et al., 2010; Xing and Jianlin, 2010; Zheng, 2011), which began to be gradually integrated into the stability verification of tunneling projects. Among them, Zheng (2008) first introduced the strength reduction method into the stability calculation of tunnel engineering, and used the safety factor calculated by the strength re-duction method as the judgment condition for the instability of the surrounding rock, and showed that this judgment condition has a strict mechanical basis and is not influenced by other factors, which can form the same standard. Huang et al. (2016) introduced the strength reduction method and solved the upper limit solution of the overall safety factor of shallow buried tunnels under complex conditions, verifying its rationality and accuracy. Additionally, a number of scholars have applied the strength reduction method to tunnel engineering and verified its applicability (Yang and Huang, 2009; Xia et al., 2012; Espada et al., 2018; Shiau and Asadi, 2020), which provides a novel tool for tunnel stability analysis in this paper.

Based on the considerations mentioned above, this paper introduces the intensity reduction method to analyze the stability of the tunnel face in sand-cobble formations. Firstly, the block shape of the rock under random conditions was considered, and a random model of sand-cobble mixture was established. Numerical simulation methods were used to conduct numerical calculations for the triaxial compression test of sand-cobble mixture, and the influence mechanisms of different confining pressures and stone contents on the mechanical properties of the sand-cobble mixture were quantitatively studied, providing parameters for engineering-scale simulations. Then, using the FLAC3D finite element simulation method, tunnel excavation models with different stone contents, tunnel depths, and different tunnel diameters were established. The safety factor was used as the evaluation index for the stability of the tunnel face, and the variation of the active failure safety factor of the tunnel face under various factors was analyzed. Based on the safety factor of the tunnel under different working conditions and the analysis of the changes in the tunnel face caused by excavation under different working conditions, this paper reveals the impact of various factors on the stability of the tunnel face in sand-cobble stratum. The research results of this paper can further improve the stability evaluation mechanism of the tunnel face in sand-cobble tunnels, and provide references for predicting the instability and failure of the tunnel face in sand-cobble tunnels.

2 Numerical modelling of the sandy cobble stratum

2.1 Study on the mechanical properties of sandy cobble stratum

Figure 1 shows a schematic diagram of the deformation prediction of the sand-cobble stratum. As illustrated, the sand-cobble stratum is a soil-rock mixture composed of high-strength cobble with varying sizes and low-stiffness fine-grained soil, and its deformation characteristics

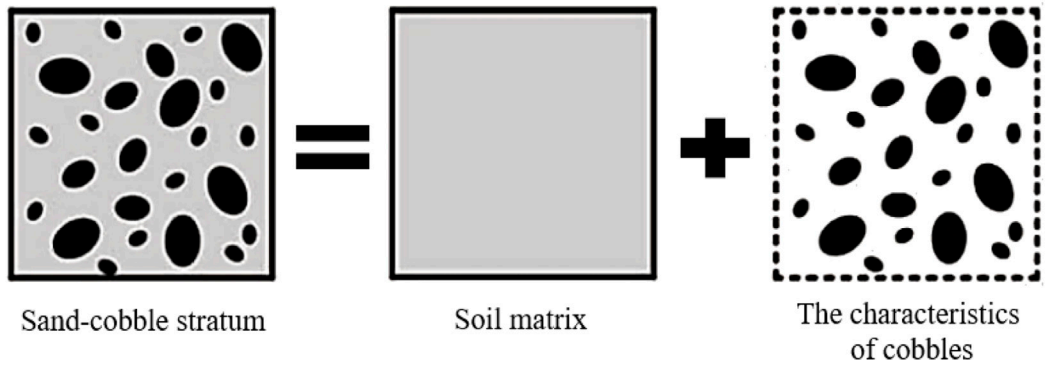

FIGURE 1
Deformation prediction method of sand-cobble stratum.

are related to the micro-structural properties of the cobble and the soil matrix. In previous studies, the stone content has been identified as an important micro-structural property that affects the mechanical properties of the sand-cobble soil (Jian et al., 2016). Hall (1951) first conducted large-scale triaxial tests on SRMs to investigate their shear strength and found that the shear strength of SRMs increases with an increase in stone content. Similar conclusions were obtained by many scholars in subsequent experiments (Lindquist, 1994; Iannacchione and Vallejo, 2000; Jafari and Shafiee, 2004; Xue et al., 2012). Based on the physical and mechanical properties of the sand-cobble soil, the failure and deformation problems of the sand-cobble soil can generally be classified into two categories: small deformation problems dominated by stress (such as triaxial compression tests), and large deformation problems dominated by particle flow (such as sand-cobble tunnel excavation problems). When studying the large deformation problems caused by tunnel excavation in sandy cobble strata, it is necessary to consider the mechanical properties of the sand-cobble mixture itself. Namely, by studying the deformation laws of the sand-cobble mixture dominated by stress to provide parameters for numerical simulation of tunnel excavation.

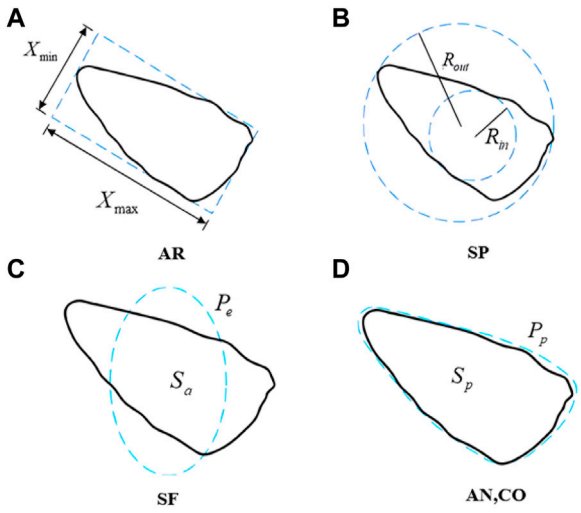

FIGURE 2
Schematic diagram of the evaluation indexes **(A)** AR, **(B)** SP, **(C)** SF and **(D)** AN, CO for the overall shape characteristics of the rock.

2.2 Construction of pebble block profile database

As mentioned above, the stone content of the sandy cobble stratum plays an important role in its stability due to its high mineral content. In order to accurately simulate the mechanical properties and kinematic characteristics of the sandy cobble stratum, this scenario requires and emphasizes the significance of better constructing a block model with similar particle size composition and random block morphology to the actual rock and soil, particularly when conducting numerical simulation tests. Firstly, the actual surface contour of the block is obtained by digital photography and digital image processing, and the shape of the block is counted. In this process, the block is equivalent to an ellipse. The laws of the long axis ratio, inclination angle and gradation of the block are obtained. In addition, a block contour shape library is established.

Mollon and Zhao's research has demonstrated that Fourier descriptors can be utlized to depict the shape of particles (Mollon and Zhao, 2012), enabling the quantitative generation of blocks with particular shape features. In this section, the two-dimensional shape features of blocks will be analyzed from a quantitative perspective based on the discrete Fourier Transform, and a two-dimensional block database will be established. Firstly, the shape features of blocks need to be studied. In previous research, Barrett proposed three-level shape index analysis methods, describing the shape of a block in a way from overall, local to detailed (Barrett, 1980). This paper will adopt Barrett et al.'s approach to analyze the shape information features of blocks at three levels. The first level describes the overall shape form, with corresponding indicators including flatness (AR) and sphericity (SP); the second level describes local roundness, with corresponding indicators including angle number (AN), convexity (CO) and shape factor (SF); the third level is the degree of roughness of surface texture, with corresponding indicators including roughness (RO). The expression method is shown in Figure 2.

They can be expressed by Eqs 1–6

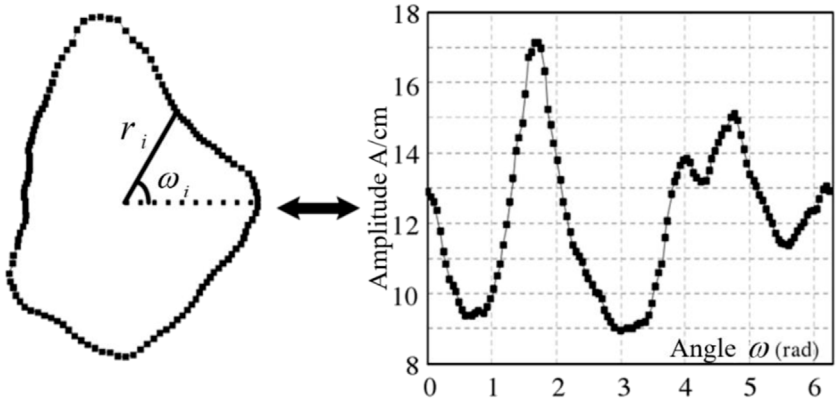

FIGURE 3
Transformation of block outlines and discrete signals.

$$AR = \frac{X_{\min}}{X_{\max}} \tag{1}$$

$$SP = \frac{R_{in}}{R_{out}} \tag{2}$$

$$AN = \frac{P_e}{P_p} \tag{3}$$

$$CO = \frac{S_a}{S_p} \tag{4}$$

$$SF = \frac{2\sqrt{\pi S_a}}{P_a} \tag{5}$$

$$RO = \frac{P_p}{P_a} \tag{6}$$

where, $X_{\max}$ and $X_{\min}$ are the maximum and minimum values of the length of the block, R_{out} is the maximum value of the radius of the inner tangent circle of the block, and R_{in} is the minimum value of the radius of the outer circle of the block. P_e denote the perimeter of the ellipse with the same area as the block, P_p and S_p are denote the perimeter and area of the smallest outer convex polygon of the block, S_a and P_a are denote the values of the area and perimeter of the block respectively.

Figure 3 depicts the transformation of the block contour with the discrete signal. As shown in Figure 3, the two-dimensional block center coordinates are $O(x_0, y_0)$, the block contour can be divided into N segments based on the center point according to equal angles ω, and the angles can be numbered as ω_1, ω_2, ω_3, $\omega_4 \ldots \omega_n$. The intersection of the corner edges with the block contour boundary is a sampling point P_i, and the distance from the center point P_i is r_1, so the position of each discrete point on the block boundary can be represented by the angle ω_i and the length of the point r_i. As a result, the length is expressed in terms of how far it is from the centroid.

The equation is expressed as follows:

$$r_i = f(\omega_i) \tag{7}$$

According to the right-angle coordinate system:

$$\begin{cases} x_i = x_0 + r_i \cos(\omega_i) \\ y_i = y_0 + r_i \sin(\omega_i) \end{cases} \tag{8}$$

Using the discrete Fourier inverse transform for the reconstruction of the block, r_i is the distance from P_i to the central point O, which can be considered as a discrete time-domain signal and expressed in terms of the Fourier series as:

$$r_i = r_0 + \sum_{n=1}^{N/2} [A_n \cos(n\omega) + B_n \sin(n\omega)] \tag{9}$$

$$r_0 = \frac{1}{N} \sum_{i=1}^{N} r_i \tag{10}$$

where, r_0 is the average radius of the block, chosen $N = 2^7 = 128$, then the block contour consists of 128 scatter points. Das N found that the higher order harmonics with ordinal number greater than $N/2$ have high frequency and low impact (Das N 2007), therefore, the total number of harmonics is chosen as $N/2$ in this paper. After polarization with reference to formula (9) and normalization (dividing both sides simultaneously by r_0), we can get:

$$\frac{r_i}{r_0} = 1 + \sum_{n=1}^{N/2} \left[\frac{\sqrt{A_n^2 + B_n^2}}{r_0} \sin(n\omega_i + \varphi_n) \right] \tag{11}$$

where, D_n is defined as the Fourier descriptor, the expression of D_n is:

$$D_n = \frac{\sqrt{A_n^2 + B_n^2}}{r_0} \ (1 \le n \le 64, n \in N^*) \tag{12}$$

Figure 4 illustrates the flowchart of the Python implementation of the discrete Fourier inverse transform for reconstructing two-dimensional rock blocks. To generate a stochastic model of soil-rock mixtures with varying stone content, a block surface morphology library and a stone content rate should be leveraged. Figure 5 displays the stochastic model generation process based on the aforesaid block surface morphology library and stone content rate.

2.3 Modelling

Under the conditions of a triaxial compression test, sandy cobble stratum belongs to the category of small deformation. Based on the assumption of small deformation continuity, the unit size of the

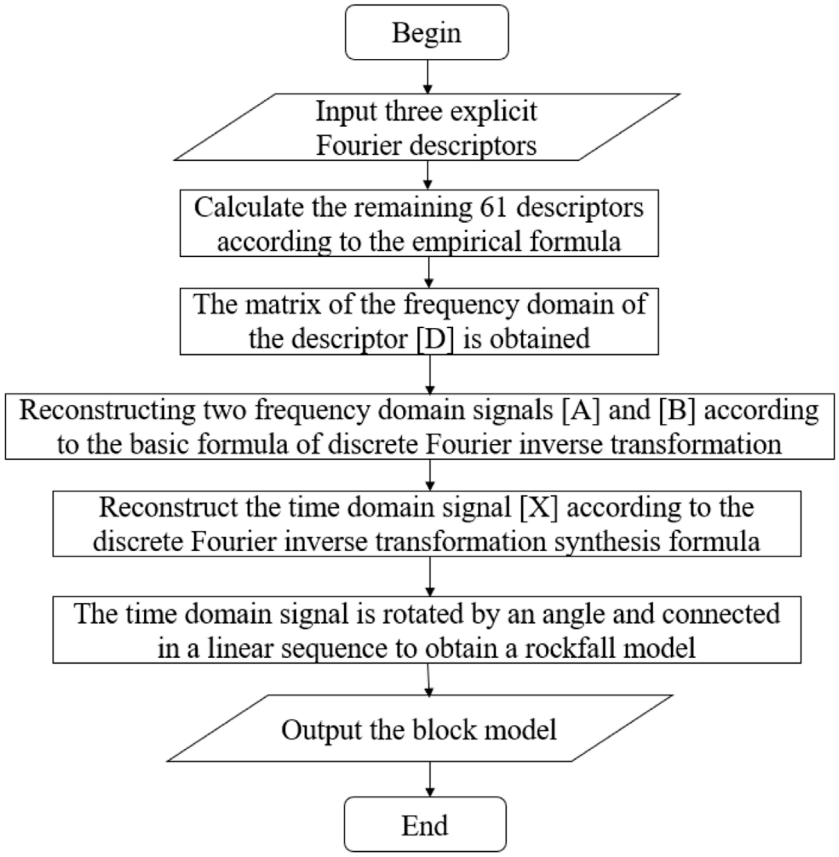

FIGURE 4
Process of obtaining a block model.

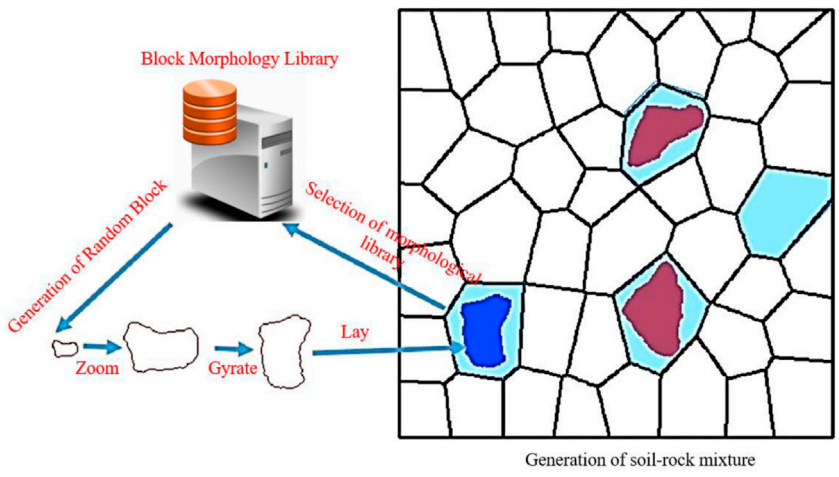

FIGURE 5
Generation of stochastic model of soil-rock mixture.

sandy is generally arbitrary. According to the engineering background of the project, the model of this test is a cylinder with diameter B) 400 mm and height H) 800 mm, and a hexahedral unit is used for free mesh division, and the mesh size is 0.005–0.01 m. In previous studies, Medley and Goodman (1994) proposed that the soil-stone threshold can be defined as:

TABLE 1 Material parameters of elements.

Soil type	Material properties	Input values
Sandy	Young's modulus of bolt (MPa)	32
	ν	0.33
	c (MPa)	0.022
	φ (°)	23
Cobble	Young's modulus of bolt (MPa)	8000
	ν	0.22
	c (MPa)	0.75
	φ (°)	38
	Tensile strength (MPa)	0.06

$$d_s = 0.05L_c \tag{13}$$

where, d_s is the soil and rock threshold, L_c is the engineering characteristic scale of soil and stone mixture.

For the triaxial test specimen, the radius is taken as the specimen, so the soil and rock threshold in this paper is 10 mm. In order to improve the calculation efficiency, this paper simplifies the soil and rock body to a certain extent, simplifying the soil particles into spheres and the block particle size into a normal distribution within 30–70 mm. Note that the particle size here is not the actual particle size of the rock block, but the equivalent particle size with the same volume of the sphere. When the particle size range of any unit sphere is 8–10 mm, it is defined as the sandy property; when the particle size of any unit polyhedron is in the range of 30–70 mm, the polyhedron is designated as the cobble property. The contact interface of the soil and rock unit is discretized and the contact interface model is established. The test adopts displacement control loading, rigid plate is set on the surface of the specimen and appropriate loading speed is set, and the bottom surface is set with fixed displacement boundary. Radial pressure boundary is adopted in the circumferential direction to simulate the surrounding pressure, and 0.1, 0.2, 0.3 and 0.4 MPa are set for four kinds of surrounding pressure respectively. According to the field survey report, the unit parameters are set as shown in Table 1.

According to the above discussion, the strength of sandy cobble soil is determined by the block stone and the soil matrix. When the stone content is small, the strength of the sandy cobble soil is determined by the soil itself, and when the stone content is too much, the strength of the sandy cobble soil is determined by the skeleton formed by the rock block. In order to better clarify the change in the shear strength of the sandy cobble stratum under different stone content conditions, numerical models with too high stone content should not be selected. In this paper, the method of establishing the block stone database in Sect. 2.2 is adopted in numerical simulation, and five different forms of stone content are selected, which are set to 0, 10%, 20%, 30% and 40%. Figure 6A,B are the numerical model of triaxial test and the random models of sandy cobble soil with five different stone contents.

2.4 Experimental results and analysis of influencing factors

2.4.1 Validation for numerical tests

To ensure the applicability and reliability of numerical models in practical engineering, it is necessary to validate the results of numerical experiments. Considering the constraints imposed by practical factors, validation can be performed by utilizing existing numerical experimental results. In this paper, taking the test results with 40% stone content and 0.2 MPa confining pressure as an example, the stress-strain relationship curve was derived, as shown in Figure 7. The deformation process of the sample was divided into three stages: the first stage was the linear elastic stage, the deviatoric stress increased with the axial strain and had a linear relationship, which increased from $0.203 \times 10^6 Pa$ to $0.523 \times 10^6 Pa$; the second stage was the elastic-plastic stage, the deviatoric stress increased from $0.523 \times 10^6 Pa$ to $0.534 \times 10^6 Pa$ with the strain increased, the overall growth rate dropped sharply, and the curve had an inflection point; the third stage was the ideal plastic stage, the deviatoric stress was basically unchanged with the increase of strain, fluctuating between $0.533 \times 10^6 Pa$ and $0.535 \times 10^6 Pa$. The results were basically consistent with the typical stress-strain curves of sand-cobble soil triaxial test in previous studies (Jiang et al., 2015). Therefore, it can be concluded that the three-axis numerical test proposed in this paper can accurately reflect the deformation characteristics of sandy cobble soil.

2.4.2 Calculation method of cohesion and angle of internal friction

The shear strength of cohesive soil depends on the cohesive force and friction between soil particles. For the shear strength of weakly cemented sandy cobble mixtures, it is usually expressed by the cohesive force c and the internal friction angle φ. Therefore, it is of great importance to solve the shear strength parameters when exploring the influence of stone content on the mechanical properties of sandy cobble soil. According to Guo et al. (2018), this study proposes a method for calculating the mechanical parameters of sand-cobble mixtures by plotting Mohr circles of the effective stress at failure.

As a result of a set of triaxial tests, all the Mohr's circles cannot be exactly tangent to the same tangent line; however, there has to be a common tangent line between two non-nested circles in the set. By finding the tangent points of all the Mohr's circles two by two, and finally by calculating the least squares equation for all the tangent points, we can obtain the envelope equation and the shear strength parameters. According to the illustration shown in Figure 8.

Mohr's circles $(\sigma_{11}, \sigma_{13})$, $(\sigma_{21}, \sigma_{23})$ have the following characteristics:

$$O_i = (\sigma_{i1} + \sigma_{i3})/2 \tag{14}$$

$$R_i = (\sigma_{i1} - \sigma_{i3})/2 \tag{15}$$

where, σ_{i1} is the maximum principal stress of the ith specimen, σ_{i3} is the minimum principal stress of the ith specimen, O_i is the coordinate of the center of the ith Mohr's circle, and R_i is the radius of the ith Mohr's circle.

Based on the geometric relationship equation:

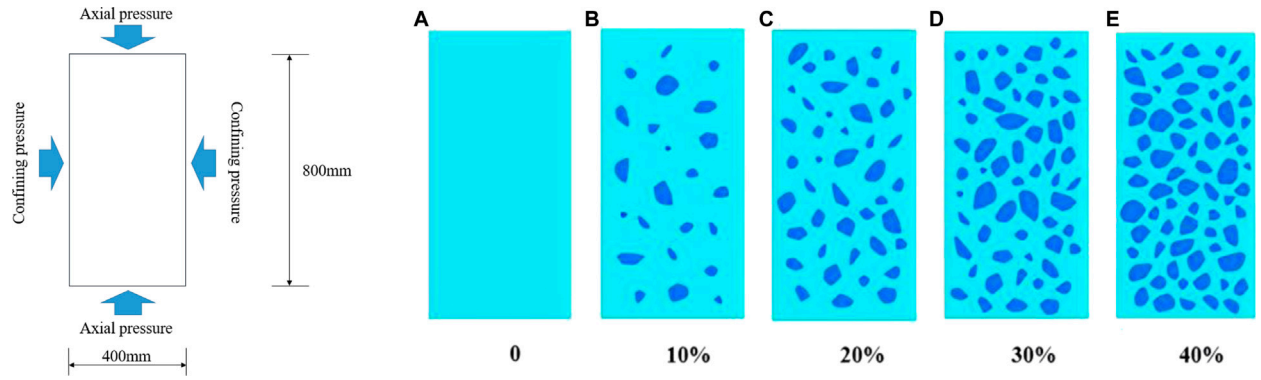

FIGURE 6
Numerical model of triaxial test and sandy cobble soil random models with different stone contents of **(A)** 0, **(B)** 10%, **(C)** 20%, **(D)** 30% and **(E)** 40%.

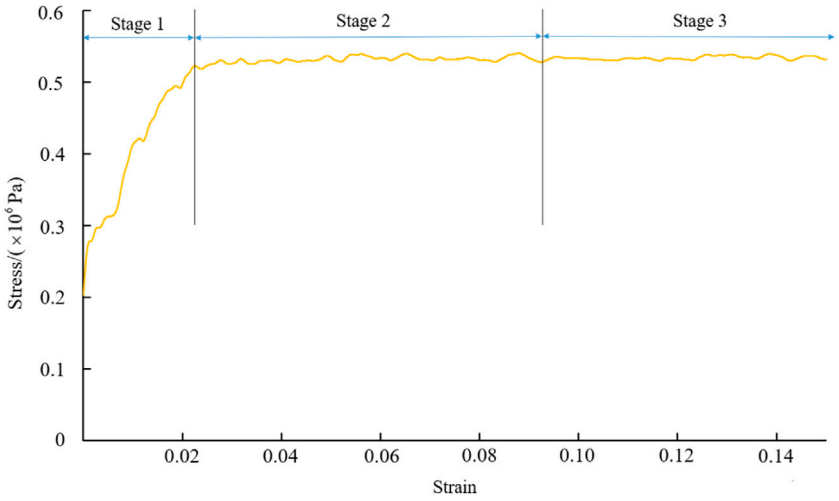

FIGURE 7
Typical deviation of stress-strain curve.

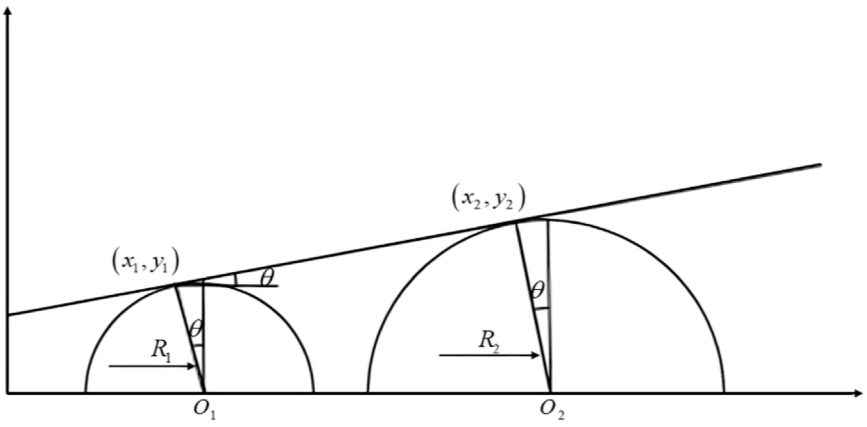

FIGURE 8
Common tangent line and its points coordinates of two cycles.

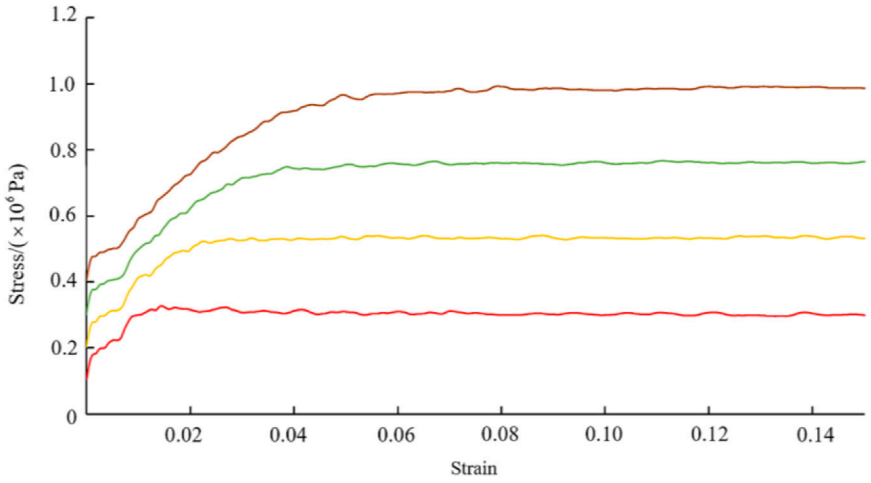

FIGURE 9
Deviation curves of stress versus strain under different confining pressures.

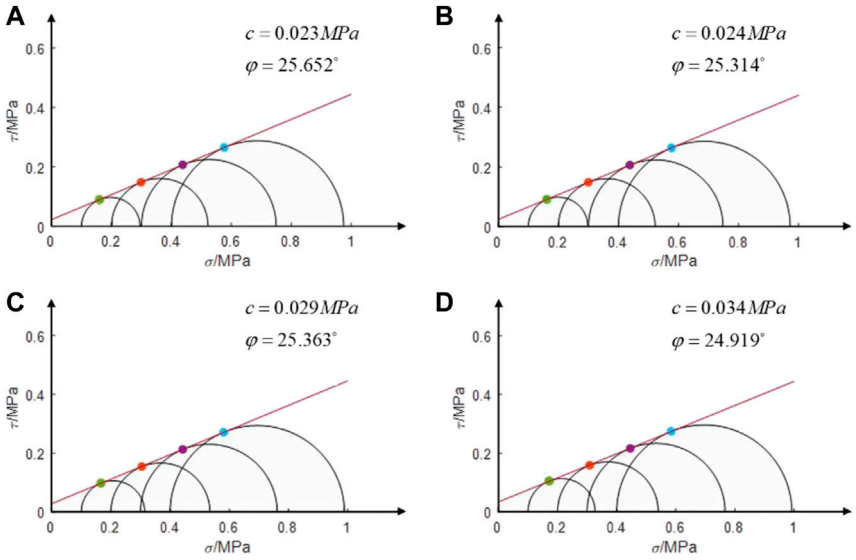

FIGURE 10
Curves of Mohr's circle with different stone contents of **(A)** 10%, **(B)** 20%, **(C)** 30% and **(D)** 40%.

$$\left.\begin{aligned} x_1 &= O_1 - R_1 \sin\theta \\ y_1 &= R_1 \cos\theta \end{aligned}\right\} \quad \left.\begin{aligned} x_2 &= O_2 - R_2 \sin\theta \\ y_2 &= R_2 \cos\theta \end{aligned}\right\} \tag{16}$$

where, x_1、 x_2、 y_1、 y_2 are the horizontal and vertical coordinates of the tangent point of the tangent line to the circle in Figure 8 respectively.

From geometric analysis there is:

$$y = \tan\theta(x - x_1) - y_1 = \tan\theta(x - x_2) - y_2 \tag{17}$$

The following equation can be obtained from Eqs 16, 17:

$$\theta = \arcsin\frac{R_2 - R_1}{O_2 - O_1} \tag{18}$$

Similarly, the coordinates of the tangent points of any two tangent lines can be determined:

$$\left.\begin{aligned} x_j &= O_j - R_j - \frac{R_k - R_j}{O_k - O_j} \\ y_j &= R_j - \cos\left[\arcsin\left(\frac{R_k - R_j}{O_k - O_j}\right)\right] \end{aligned}\right\} \tag{19}$$

$$\left.\begin{aligned} x_k &= O_k - R_k - \frac{R_k - R_j}{O_k - O_j} \\ y_k &= R_k - \cos\left[\arcsin\left(\frac{R_k - R_j}{O_k - O_j}\right)\right] \end{aligned}\right\} \tag{20}$$

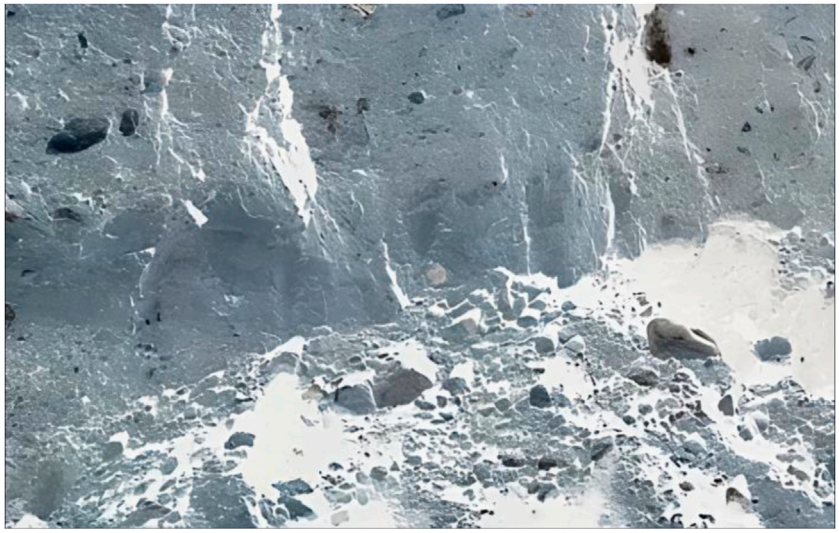

FIGURE 11
Sandy cobble stratum.

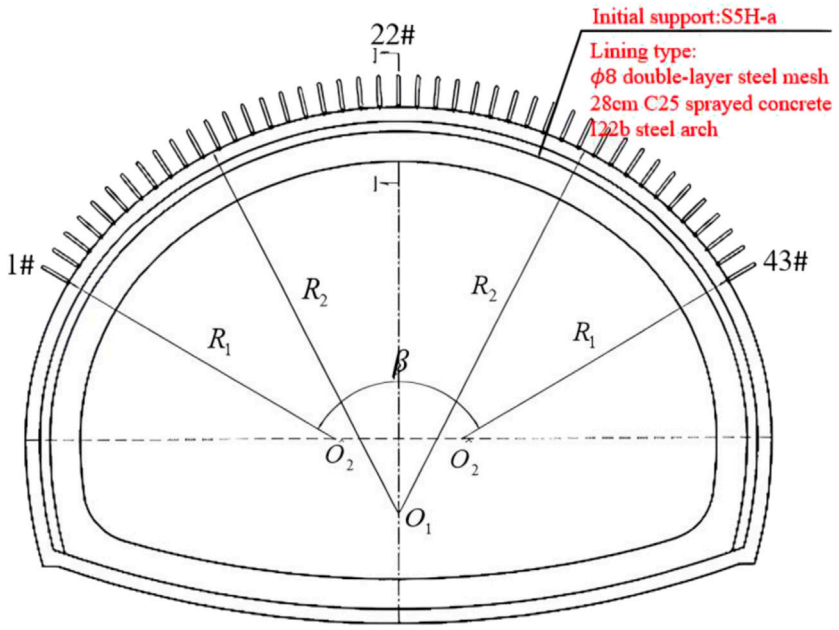

FIGURE 12
Tunnel profile and support parameter.

Assume that there are k trials in a series of triaxial tests, and that tangent two to two will give us the total number of tangent points m in the series of triaxial tests:

$$m = 2 - C_k^2 = k - (k - 1) \tag{21}$$

For fitting a curve, one should derive its most general n-polynomial fit, which assumes that its most general curve expression is:

$$S(x) = a_0 + a_1 x + \cdots + a_n x^n = \sum_{i=1}^{n} a_i x^i \tag{22}$$

According to the principle of least squares:

$$I(a_0, a_1, \ldots, a_n) = \sum_{j=1}^{m} \left[\sum_{i=0}^{n} \left(a_i x_j^i - y_j \right)^2 \right] \tag{23}$$

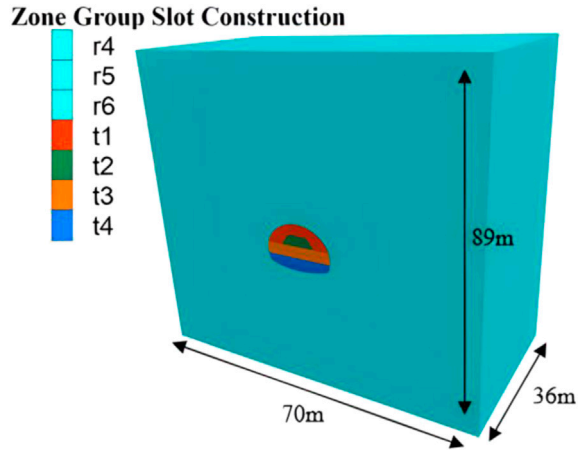

FIGURE 13
Numerical model for the analysis of tunnel face stability.

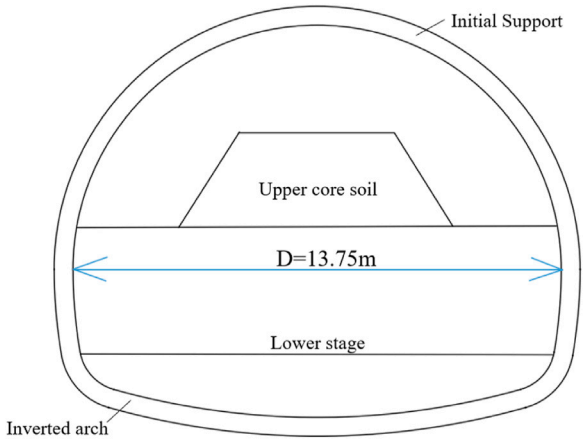

FIGURE 14
Cross-section of tunnel in numerical test.

TABLE 2 Strength and deformation parameters of samples with different stone content.

Stone content (%)	E (MPa)	v	c (MPa)	φ (°)
10	37.78	0.32	0.023	25.652
20	46.62	0.31	0.024	25.314
30	57.08	0.28	0.029	25.363
40	68.94	0.26	0.034	24.919

The problem of finding the extreme value of I function on $a_0, a_1, \ldots, a_n$, from the necessary conditions for the extreme value of a multivariate function, there is:

$$I(a_0, a_1, \ldots, a_n) = 2\sum_{j=1}^{m}\left[\sum_{i=0}^{n}\left(a_i x_j^i - y_j\right)\right]x^i = 0, i = 0, 1, \ldots, n \quad (24)$$

$$c_{pq} = \sum_{j=1}^{m} x_j^p x_j^q \quad (25)$$

$$b_p = \sum_{j=1}^{m} x_j^p y_j \quad (26)$$

According to Eq. 24, there is:

$$C - A = B \quad (27)$$

where: p、$q \in (0, 1, 2, \ldots, n)$; $A = (a_0, a_1, \ldots, a_n)^T$; $B = (b_0, b_1, \ldots, b_n)^T$; $C = \begin{pmatrix} c_{00} & \cdots & a_{0n} \\ \vdots & \ddots & \vdots \\ c_{n0} & \cdots & a_{nn} \end{pmatrix}$.

Eq. 27 can theoretically be fitted to the molar envelope of any number of polynomials, and the coefficients a_0, a_1 of the envelope Equation $y = a_0 + a_1 x$ can be determined from Eq. 27 to obtain the shear strength parameters:

$$\left.\begin{array}{l} c = a_0 \\ \varphi = \arctan a_1 \end{array}\right\} \quad (28)$$

2.4.3 Influence of confining pressure and stone content

This paper adopted four confining pressures of 0.1 MPa, 0.2 MPa, 0.3 MPa and 0.4 MPa respectively, keeping the confining pressure constant and increasing the axial pressure step by step until the sample was damaged. Taking the unit size of 0.01 m and 40% stone content, the stress-strain relation curves of the samples under different confining pressures σ_3 were obtained as shown in Figure 9. It can be observed from the figure that with the increase of confining pressure, the peak strength of the sample increases and the linear elastic stage prolongs, but the change of confining pressure does not affect the timing of the sample entering the ideal stage.

Under the condition of a 0.05 m unit size, specimens with different stone contents (0%, 10%, 20%, 30%, and 40%) were prepared and tested under various confining pressures. The Mohr stress circles obtained from the numerical simulation of the triaxial tests on the sand-cobble mixtures with different stone contents are presented in Figure 10. The strength envelopes exhibit a typical linear trend. Using the method described in Section 2.4.2 to calculate the shear strength parameters c and φ, the shear strength indicators of sand-cobble mixtures with different stone contents are shown in Table 2. The shear strength parameter values c of different grading types show a slow increasing trend with increasing stone content. However, the value φ of the parameter does not show an obvious increasing trend and remains within the range of 24.9° to 25.7°, with a general increasing trend in shear strength. For weakly cemented rock masses like sand-cobble mixture, the shear strength is mainly determined by the interaction of soil and rock blocks. When the stone content is low, the strength parameter of the mixture is mainly determined by the soil. As the stone content increases from 0% to 40%, the proportion of rock on the shear surface becomes larger, and the possibility of shear damage in sand-cobble stratum decreases at this time. At the same time, the increase in stone content enhances the strength of the soil, and during the triaxial compression process, the sand-cobble mixture becomes more compact as a whole, thus increasing the cohesion between the soil particles.

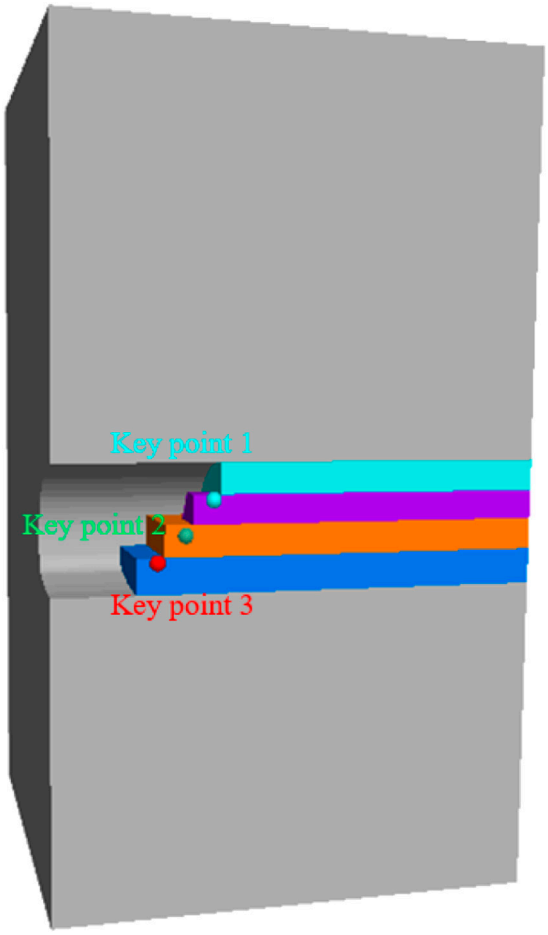

FIGURE 15
The location of key points.

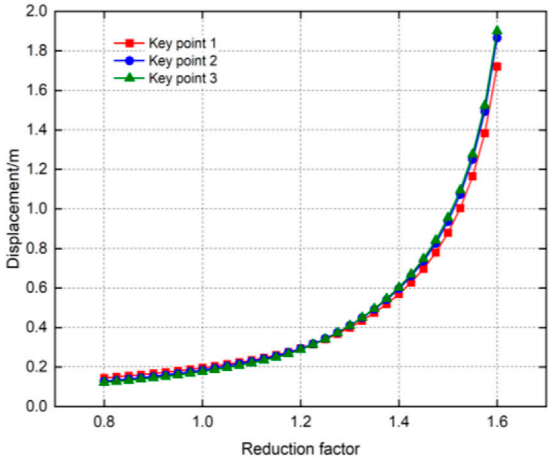

FIGURE 16
Fitting curve of displacement of the key point vs reduction coefficient.

3 Numerical modelling of the tunnel face stability

3.1 Project overview

The Da Zhuang Tunnel is located in Xishan Village, Donggou Township, Huzhu Tu Autonomous County, Qinghai Province, which is a separated middle tunnel. The left line starts from ZK40+366 to ZK40+960, with a length of 594 m, and the right line starts from YK40+454 to YK41+126 with a length of 672 m. The portal section is mainly composed of sand-cobble strata (Figure 11), which is gray and yellow soil, medium density, mostly cobble, filled with sand and fine clay. The cobble size and shape are irregular, which greatly impacts the tunnel. After tunnel construction, the construction party adjusted the design parameters according to the actual geological conditions. Initial support was S5H-a, and the lining type was C22 drug roll anchor single 4 m (radial space 100 cm, vertical 50 cm) + φ 8 double-layer steel mesh (20 × 20 cm) + spacing 50 cm I22b steel arch +28 cm C25 sprayed concrete. The main support and lining parameters are shown in Figure 12. After the scheme comparison, the step method was adopted for excavation.

3.2 Numerical model description

In accordance with the actual engineering situation of the project, the stepwise method is adopted in this paper, taking the arc guide pit excavation and reserving the core soil as the basic model, with three steps and seven excavation faces. The excavation and support at each position are staggered and parallel along the tunnel. To study the stability of the face during the excavation of sand-cobble tunnel, FLAC3D is used for numerical simulation. Figure 13 shows the calculation model of sandy cobble tunnel with a burial depth of $H = 30m$. The model size is $70m \times 36m \times 89m$. Note that the top soil layer thickness is different for different burial depths. Ignoring the influence of boundary adjustment on the analysis, 3D non-uniform mesh is used, with mesh size of 0.5–2.0 m, all of which are hexahedral mesh. The model is composed of about 69,288 regions (the term "region" is the term of each discrete unit in FLAC3D). In the numerical simulation process, the lining is not considered, and it is assumed that the tunnel excavation around is fixed boundary. Therefore, the boundary conditions are set as follows: normal constraints are applied to the upper, the lower and side surfaces. The cross-sectional micro-view analysis model of tunnel excavation is shown in Figure 14, with the maximum span of the tunnel diameter D as 13.75 m and the burial depth H as 30 m. Since the tensile strength and compressive strength of the boulder are relatively large, it usually does not fail under the action of tunnel excavation load, so it can be regarded as elastic material. The mechanical properties and deformation behavior of the soil matrix are described by the classical Mohr-Coulomb elastic-plastic constitutive model. According to the actual working conditions, the microscopic component material parameters of the sandy cobble stratum are shown in Table 1.

3.3 Simulation process

In order to ensure the stability of the face in the tunnel construction process, many scholars have studied the factors

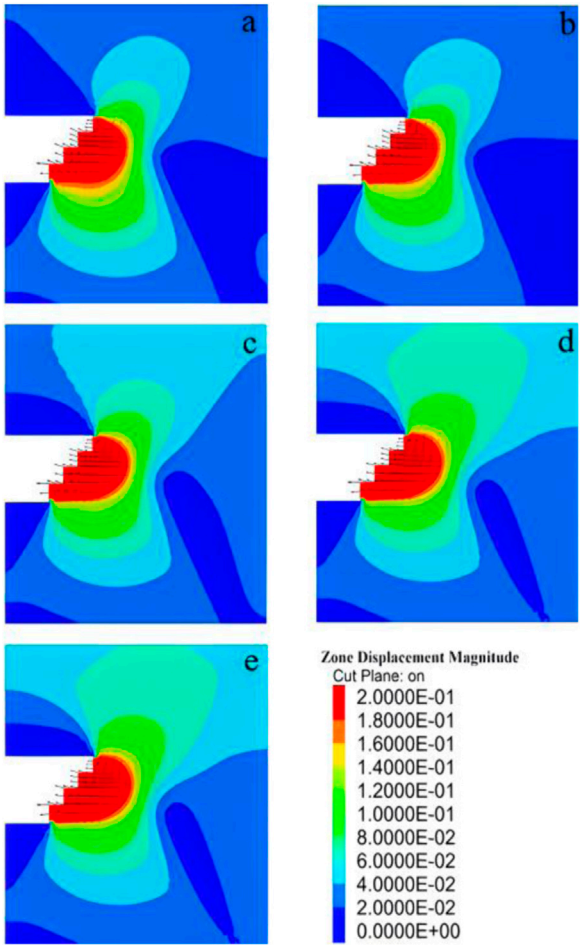

FIGURE 17
Displacement nephogram in front of tunnel face with different stone contents of **(A)** 0, **(B)** 10%, **(C)** 20%, **(D)** 30% and **(E)** 40%.

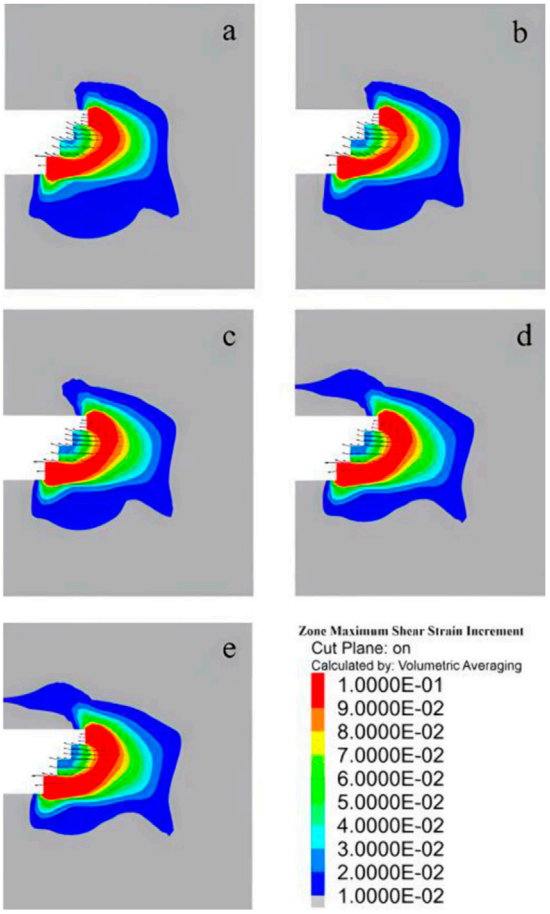

FIGURE 18
Stress nephogram with different stone contents of **(A)** 0, **(B)** 10%, **(C)** 20%, **(D)** 30% and **(E)** 40%.

influencing the stability of the face through numerical simulation. The main influencing factors leading to the deformation of the face are relatively high stress and poor geological conditions, and the relationship between stress and burial depth is relatively large, so the burial depth of the tunnel is the main factor affecting the stability of the face (Chen et al., 2013; Liu et al., 2019; Li et al., 2022). The ultimate support pressure of the face is the key factor to ensure the stability of the face. Li used FLAC3D to numerically analyze the critical support pressure of the face in the tunnel, and found that the diameter of the excavation surface was also important for the stability of the face in the process of tunnel excavation (Li et al., 2022). According to the conditions of the sandy cobble stratum tunnel, the stone content is an important factor affecting the stability of the sandy cobble soil, so the large deformation problem of the face caused by the excavation of tunnel is related to the stone content in sandy cobble stratum. Based on the above discussion, in the stability analysis of the face in sandy cobble stratum tunnel, the influence of stone content, tunnel burial depth and tunnel diameter should be considered comprehensively. This paper will analyze in detail according to the following three working conditions:

Condition 1: The stone content of the sandy cobble soil is the variable, while the tunnel depth and tunnel diameter are the constants. Calculate according to the stone content of the core soil, which are 0%, 10%, 20%, 30%, and 40%, the tunnel depth is 30m, and the tunnel diameter is 13.75 m, to study the influence of the stone content on the stability of the tunnel face in sandy cobble stratum.

Condition 2: The tunnel depth is the variable, while the stone content and tunnel diameter are the constants. Calculate according to the tunnel depth, which are 10 m, 20 m, 30 m, 40 m, and 50 m, the stone content is 10%, and the tunnel diameter is 13.75 m, to study the influence of the tunnel depth on the stability of the tunnel face in sandy cobble stratum.

Condition 3: The tunnel diameter is the variable, while the stone content and tunnel depth are the constants. Calculate according to the tunnel diameter, which are 11.75 m, 12.75 m, 13.75 m, 14.75 m, and 15.75 m, the stone content is 10%, and the depth of tunnel is 30 m, to study the influence of the chamber size on the stability of the tunnel face in sand-cobble stratum.

3.4 Analysis of safety factor of tunnel face stability

The analysis of tunnel face stability is a three-dimensional problem. Although numerical simulation analysis technology can

TABLE 3 Safety factors with different stone content, buried depth and tunnel diameter.

Factors	Values	Safety factors
Stone content (%)	0	1.15
	10	1.3
	20	1.375
	30	1.525
	40	1.65
Buried depth m)	10	1.75
	20	1.525
	30	1.3
	40	1.15
	50	1.025
Tunnel diameter(m)	11.75	1.4
	12.75	1.375
	13.75	1.3
	14.75	1.25
	15.75	1.175

simulate the whole construction process and the damage mechanism of the face, it is difficult to obtain the safety factor of the tunnel face support in time due to its poor temporality, which is not conducive to the judgment of the stability of the tunnel face during construction and the overall control of the project (Jiang et al., 2015). The safety factor obtained by the strength reduction method not only can describe the relative quantity relationship between the strength of the tunnel face and the secondary stress caused by excavation, and the overall resistance of the tunnel face to the secondary stress, but also can characterize the shear stability of the face. Therefore, the safety factor can be used as an important index for the overall safety evaluation of the tunnel.

The strength reduction method was first proposed by Bishop (1955), which defined the strength reduction coefficient as the ratio of the existing shear strength of the soil to the shear strength required to maintain equilibrium. The principle is to divide the soil parameters (c, φ) by the reduction coefficient at the same time to obtain a set of reduced new cohesion and internal friction angle values, and then calculate according to this set of new parameters until the soil reaches the critical state of instability, at which time the corresponding reduction coefficient is the safety factor. At present, there are mainly the following instability criteria in numerical calculation for geotechnical engineering: 1) numerical calculation does not converge within the specified number of iterations; 2) the general plastic strain or general shear strain occurs overall; 3) displacement mutation occurs at characteristic points (Hoek et al., 1998). In this paper, the strength reduction method is used in FLAC finite difference software. Due to the non-uniform deformation of the tunnel face, selecting only the point with the maximum displacement may not provide a comprehensive assessment of the deformation of the tunnel. According to the Mohr-Coulomb criterion, taking into account the spatial distribution, we have chosen three characteristic points uniformly distributed on the tunnel face, and the selection location of the characteristic points is shown in Figure 15. By reducing the cohesion and friction angle according to Eqs 29, 30, and recording the change of the displacement of the three characteristic points at each step, the reduction coefficient at the time when the displacement of the three characteristic points changes suddenly is taken as the safety factor. In other word, the safety factor is judged according to the displacement change of the characteristic points.

$$c_F = \frac{c_0}{K} \tag{29}$$

$$\varphi_F = \tan^{-1}\left(\frac{(\tan\varphi_0)}{K}\right) \tag{30}$$

where, c_0, c_F are initial cohesion and limit state cohesion, φ_0、 φ_F are initial internal friction angle and limit state internal friction angle, and K is the safety factor (reduction factor).

When a numerical model with 10% stone content, 30 m tunnel burial depth and 13.75 m tunnel diameter is selected, the displacement of the test point changes with the reduction factor as the abscissa and the displacement of the key feature point as the ordinate, as shown in Figure 16. Based on the engineering geological background, we first quantify the variations in displacement at the monitoring points. We set the threshold for the slope of the curve indicating abrupt changes in displacement to 1.5. It can be seen from the figure that the reduction factor increases gradually from 0.8 and the displacement of the measuring point increases slowly with the increase of the reduction factor before reaching 1.3, which shows a linear proportional relationship between them, indicating that the tunnel face is in the elastic-plastic deformation stage and is overall stable, which can continue to bear the load. When the reduction factor increases to 1.3, the slope of the curve is 1.5, the variation rate of the displacement of the measuring point increases and enters the rapid increase stage, indicating that the tunnel face enters the unstable destruction stage and is in the quasi-limit equilibrium state. When the reduction factor is greater than 1.3, the displacement variation of the measuring point is almost parallel to the ordinate representing the deformation displacement, indicating that the tunnel face has undergone destruction.

4 Numerical modelling results and discussions

4.1 Effect of stone content

To analyze the deformation of the face under varying stone content conditions, we numerically simulated five different types of tunnels with a buried depth of 30 m, a tunnel diameter of 13.75 m, and stone contents of 0%, 10%, 20%, 30%, and 40%. Two methods, namely, the stepwise method and the core soil method, were employed under working condition 1. By statistically analyzing the deformation of the soil in front of the face caused by the different control groups, we obtained displacement cloud maps of the soil under various conditions (Figure 17). The failure pattern was extracted from the vertical cross section of the three-dimensional numerical model. As depicted in Figure 17, under the same tunnel

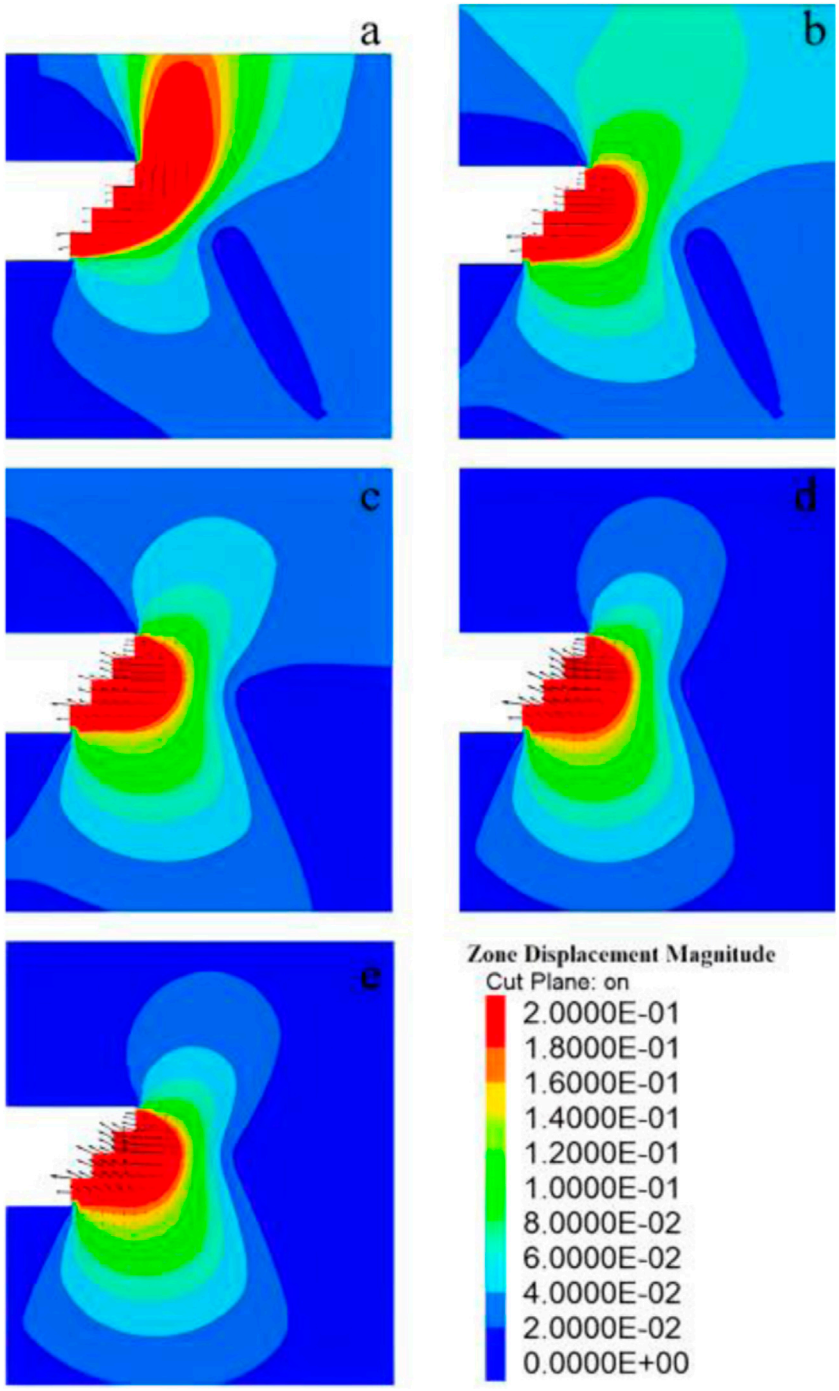

FIGURE 19
Displacement nephogram in front of tunnel face with different buried depths of **(A)** 10 m, **(B)** 20 m, **(C)** 30 m, **(D)** 40 m and **(E)** 50 m.

buried depth and diameter, the soil in front of the face exhibited the highest displacement near the semicircular region across different stone contents, which aligns with previous numerical experiments (Zhang et al., 2015).

As the stone content increased, the red area indicating maximum soil deformation in front of the face gradually decreased. Conversely, the area with minimal displacement of the upper soil in front of the face gradually increased, while the displacement of the lower soil remained relatively unchanged. Figure 18 illustrates the change in shear strain during tunnel excavation for both the face and the soil in front of it. Notably, the upper and lower steps of the face exhibited the highest shear strain. Moreover, with increasing stone content, the area with maximum shear strain at the face decreased, and the shear strain transferred from the soil below the face to the soil above it. Consequently, the stability of the tunnel face improved during excavation as observed in the figure.

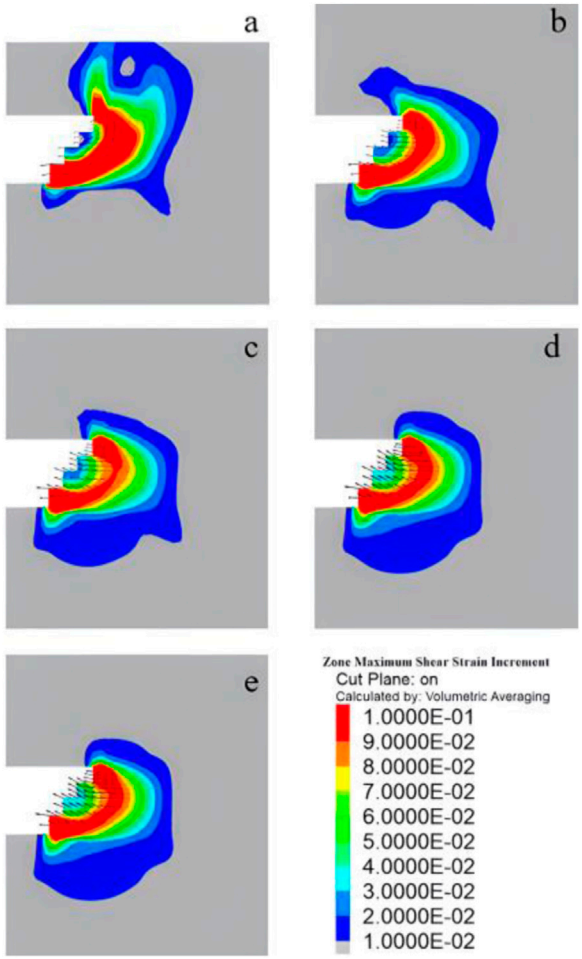

FIGURE 20
Stress nephogram with different buried depths of **(A)** 10 m, **(B)** 20 m, **(C)** 30 m, **(D)** 40 m and **(E)** 50 m.

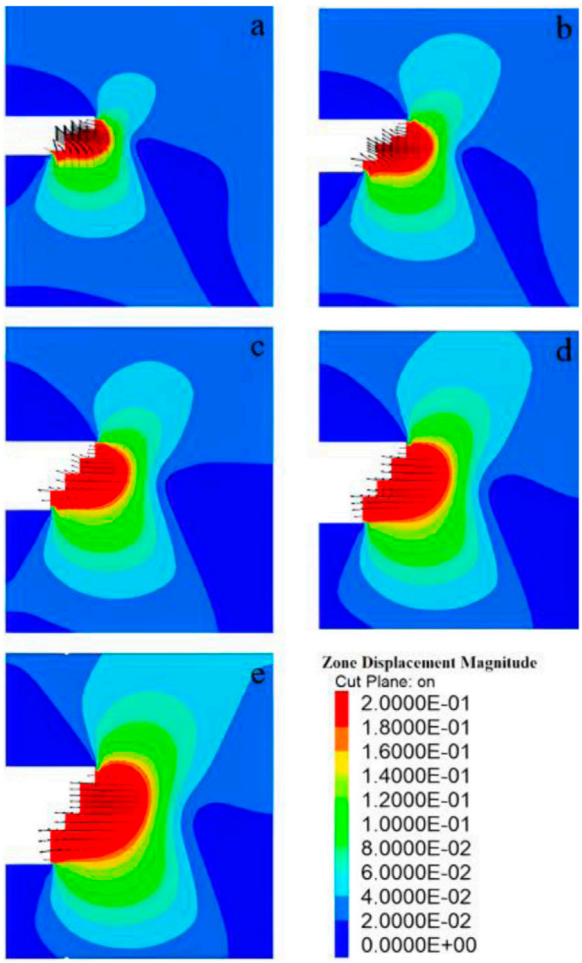

FIGURE 21
Displacement nephogram in front of tunnel face with different tunnel diameters of **(A)** 11.75 m, **(B)** 12.75 m, **(C)** 13.75 m, **(D)** 14.75 m and **(E)** 15.75 m.

Table 3 presents the safety factor values calculated using the method proposed in Section 3.3 for the sand-cobble tunnel model, with stone content ranging from 0% to 40%. It is evident that the safety factor increases with higher stone content. At 0% stone content, the calculated safety factor was 1.15, indicating an unstable and vulnerable face. However, at 40% stone content, the safety factor increased to 1.65, accompanied by reduced shear strain at the face and improved face stability. Therefore, we can conclude that, under equivalent excavation depth and chamber size, increasing the stone content in the sand and gravel stratum enhances the stability of the tunnel face during excavation.

4.2 Effect of tunnel buried depth

The buried depth of a sandy cobble stratum tunnel is a critical factor influencing the stability of the tunnel face. In Condition 2, we simulated the excavation of tunnel models with five different buried depths. These sandstone tunnel models had a stone content of 10%, a tunnel diameter of 13.75 m, and embedment depths of 10 m, 20 m, 30 m, 40 m, and 50 m respectively. By analyzing the displacement and shear strain changes in the soil in front of the tunnel face for each experimental group, we obtained displacement and shear strain change cloud maps, shown in Figure 19 and Figure 20 respectively. Figure 19 reveals that the greatest soil deformation in front of the tunnel face typically occurs at the face itself. At a buried depth of 10m, the maximum displacement of the tunnel face and the soil in front of it is concentrated in the middle and upper part of the face. As the buried depth increases, the displacement decreases in the upper part and increases in the lower part. At a buried depth of 50m, the displacement mainly occurs in the middle and lower part of the soil in front of the tunnel face. Figure 20 demonstrates that, during excavation using the step method, the highest shear strain occurs at the upper and lower steps of the tunnel face and the front of the face. With increasing buried depth, the maximum range of shear strain in front of the face gradually decreases. At a buried depth of 50 m, the maximum range of shear strain reaches a minimum, indicating that the tunnel face is most unstable and susceptible to damage at this point. Consequently, in sandy cobble tunnels with a consistent stone content and tunnel diameter, deeper buried depths result in poorer tunnel face stability during excavation.

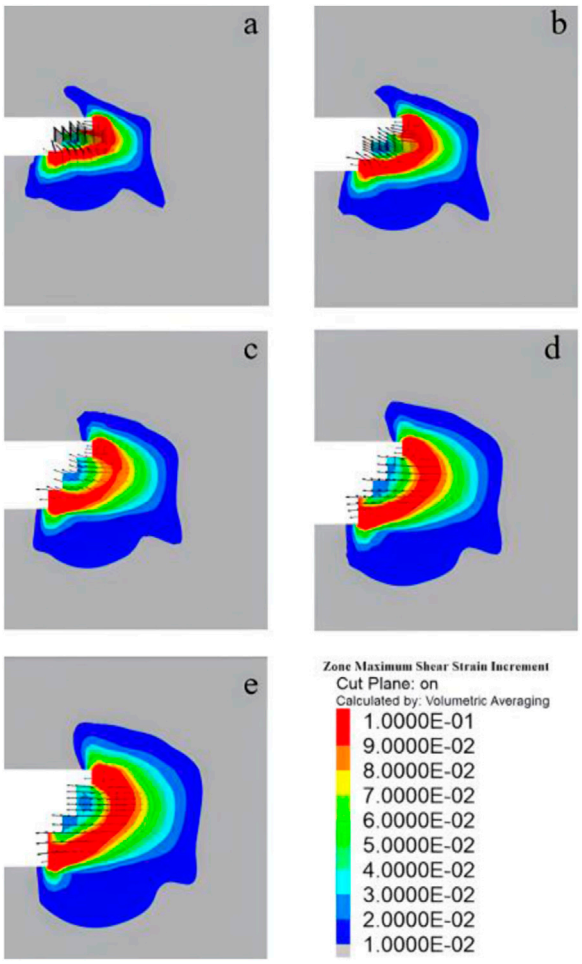

FIGURE 22
Stress nephogram with different tunnel diameters of **(A)** 11.75 m, **(B)** 12.75 m, **(C)** 13.75 m, **(D)** 14.75 m and **(E)** 15.75 m.

As shown in Table 3, when a buried depth of 10 m, the safety factor of the tunnel face is 1.75. As the buried depth increases, the safety factor progressively decreases. When the buried depth reaches 50 m, the safety factor drops to 1.025, indicating a high vulnerability of the tunnel face to damage. In conclusion, when excavating tunnels in sandstone strata with a constant stone content and tunnel diameter, the stability of the tunnel face deteriorates with increasing buried depth.

4.3 Effect of tunnel diameter

In working condition 3, simulations were conducted on tunnel models with a 10% stone content and a 30 m buried depth, with five different tunnel diameters: 11.75 m, 12.75 m, 13.75 m, 14.75 m, and 15.75 m. The displacement of the face and the soil in front of the face varied with the tunnel diameter, as depicted in Figure 21. Analysis of Figure 21 reveals that the largest displacement of the face and the soil in front of the face occurred at the tunnel diameter, while the soil above and below the face exhibited slight displacements in an elliptical shape. As the tunnel diameter increased, the displacement of the soil in the upper part in front of the face gradually increased, and the area of soil deformation in front of the face gradually expanded. Figure 22 presents the shear strain of the soil in front of the face as the tunnel diameters changed. It is evident from the figure that the shear strain of the soil in front of the face increased with the increase in tunnel diameter.

In Table 3, when the tunnel diameter was 11.75 m, the calculated safety factor of the face was 1.4. Considering the displacement and shear strain of the soil in front of the face, the stability of the face was deemed satisfactory at this point. However, as the tunnel diameters increased to 15.75 m, the safety factor of the face decreased to 1.175. At this stage, a large area of soil displacement in front of the face and significant shear strain were observed, indicating that the face became unstable and susceptible to damage during excavation. Consequently, it can be concluded that under constant stone content and buried depth conditions, the stability of the tunnel face diminishes with increasing tunnel diameters during the excavation of the sandy cobble tunnel.

5 Conclusion

Based on the inhomogeneity of the sand-cobble stratum, this paper has developed a numerical model to investigate tunnel excavation under different stone contents. The model combines numerical simulation, the finite difference program FLAC3D, and the strength reduction method to provide a more comprehensive understanding of the stability evaluation mechanism of the tunnel face in the sand-cobble stratum. The following conclusions were drawn in order to analyze the influence of various factors on the stability of the tunnel face and to examine the stability under various working conditions.

(1) When the stone content increases from 0% to 40% under the same confining pressure, the maximum shear strength of the sand-cobble soil increases accordingly. This suggests that a higher stone content in the sand-cobble stratum enhances the macroscopic strength of the material.
(2) The stability of the tunnel face can be evaluated using the strength reduction method with the characteristic point mutation criterion as the instability criterion. This method enables the calculation of the stability safety factor of the face and provides a novel approach for assessing tunnel face stability.
(3) Prior to damage, the tunnel face in the sand-cobble stratum experiences extrusion deformation, with the maximum deformation occurring in the face and the soil in front of it. The development of damage tends to initiate from the front of the face.
(4) The stone content in the sand-cobble stratum significantly affects the stability of the tunnel face. As the stone content increases, the stability of the tunnel face gradually improves. Additionally, the tunnel excavation depth and diameter have a significant impact on the stability of the tunnel face. Increasing the depth and diameter of the tunnel excavation leads to a decrease in the stability of the tunnel face.

Data availability statement

The original contributions presented in the study are included in the article/supplementary material, further inquiries can be directed to the corresponding authors.

Author contributions

HX: methodology, writing–original draft. LL: investigation, resources. XG: investigation, resources. YiZ: software, formal analysis, methodology, writing–review and editing. HW: conceptualization, methodology, supervision. All authors contributed to the article and approved the submitted version.

Funding

This research is financially supported by the Key R&D and Transformation Plan of Qinghai Province (2021-SF-167).

Conflict of interest

Authors HW, LL, and XG were employed by Qinghai Traffic Investment Co., Ltd and Qinghai Xihu Expressway Management Co., Ltd; JZ and YZ were employed by China National Logging Corporation.

The remaining authors declare that the research was conducted in the absence of any commercial or financial relationships that could be construed as a potential conflict of interest.

Publisher's note

All claims expressed in this article are solely those of the authors and do not necessarily represent those of their affiliated organizations, or those of the publisher, the editors and the reviewers. Any product that may be evaluated in this article, or claim that may be made by its manufacturer, is not guaranteed or endorsed by the publisher.

References

Augarde, C. E., Lyamin, A. V., and Sloan, S. W. (2003). Stability of an undrained plane strain heading revisited. *Comput. Geotechnics* 30 (5), 419–430. doi:10.1016/s0266-352x(03)00009-0

Barrett, P. J. (1980). The shape of rock particles, a critical review. *Sedimentology* 27 (3), 291–303. doi:10.1111/j.1365-3091.1980.tb01179.x

Bishop, A. W. (1955). The use of the slip circle in the stability analysis of slopes. *Geotechnique* 5 (1), 7–17. doi:10.1680/geot.1955.5.1.7

Chen, R. P., Li, J., Kong, L. G., and Tang, L. j. (2013). Experimental study on face instability of shield tunnel in sand. *Tunn. Undergr. Space Technol. Incorporating Trenchless Technol. Res.* 33 (Jan.), 12–21. 3. doi:10.1016/j.tust.2012.08.001

Chen, R. P., Tang, L. J., Ling, D. S., and Chen, Y. (2011). Face stability analysis of shallow shield tunnels in dry sandy ground using the discrete element method. *Comput. Geotechnics* 38 (2), 187–195. doi:10.1016/j.compgeo.2010.11.003

Das, N. (2007). *Modeling three-dimensional shape of sand grains using discrete element method[M]*. University of South Florida.

Espada, M., Muralha, J., Lemos, J. V., Jiang, Q., Feng, X. T., Fan, Q., et al. (2018). Safety analysis of the left bank excavation slopes of Baihetan arch dam foundation using a discrete element model. *Rock Mech. Rock Eng.* 51, 2597–2615. doi:10.1007/s00603-018-1416-2

Guo, X., Dias, D., Carvajal, C., Peyras, L., and Breul, P. (2018). Reliability analysis of embankment dam sliding stability using the sparse polynomial chaos expansion. *Eng. Struct.* 174, 295–307. doi:10.1016/j.engstruct.2018.07.053

Hall, E. (1951). A triaxial apparatus for testing large soil specimens. *Triaxial testing of soils and bitminous mixtures*. ASTM International.

Han, K., Zhang, C., Li, W., and Guo, C. (2016a). Face stability analysis of shield tunnels in homogeneous soil overlaid by multilayered cohesive-frictional soils. *Math. Problems Eng.* 2016, 1–9. doi:10.1155/2016/1378274

Han, K., Zhang, C., and Zhang, D. (2016b). Upper-bound solutions for the face stability of a shield tunnel in multilayered cohesive–frictional soils. *Comput. Geotechnics* 79, 1–9. doi:10.1016/j.compgeo.2016.05.018

Hoek, E., Marinos, P., and Benissi, M. (1998). Applicability of the Geological Strength Index (GSI) classification for very weak and sheared rock masses. The case of the Athens Schist Formation. *Bull. Eng. Geol. Environ.* 57, 151–160. doi:10.1007/s100640050031

Huang, F., Li, Z., and Ling, T. (2016). Upper bound solution of safety factor for shallow tunnels face using a nonlinear failure criterion and shear strength reduction technique. *Math. Problems Eng.* 2016, 1–8. doi:10.1155/2016/4832097

Huang, M., Li, S., Yu, J., and Tan, J. Q. W. (2018) Continuous field based upper bound analysis for three-dimensional tunnel face stability in undrained clay. *Comput. Geotech.* 94, 207–213.

Iannacchione, A. T., and Vallejo, L. E. (2000) Shear strength evaluation of clay-rock mixtures. *Slope Stab.* 209–223.

Jafari, M. K., and Shafiee, A. (2004). Mechanical behavior of compacted composite clays. *Can. Geotechnical J.* 41 (6), 1152–1167. doi:10.1139/t04-062

Jiang, Y., Yong, F., and He, C. (2015). Study on delayed settlement formation induced by shield tunneling in sandy cobble strata. *Chin. J. Undergr. Space Eng.*

Jian, P. J., Lu, J. F., and Zhong, Y. Z. (2016). Study on strength parameter of sandy pebble soil based on different density and moisture content. *Sci. Technol. Eng.* 16 (24), 257–261.

Kalender, A. Y. C. A. N., Sonmez, H., Medley, E., Tunusluoglu, C., and Kasapoglu, K. E. (2020). An approach to predicting the overall strengths of unwelded bimrocks andbimsoils. *IEng. Geol.* 183, 65–79.

Li, W., and Zhang, C. (2020). Face stability analysis for a shield tunnel in anisotropic sands. *Int. J. Geomechanics* 20 (5), 04020043. doi:10.1061/(asce)gm.1943-5622.0001666

Li, W., Zhang, C., Zhang, D., Ye, Z., and Tan, Z. (2022). Face stability of shield tunnels considering a kinematically admissible velocity field of soil arching. *J. Rock Mech. Geotechnical Eng.* 14 (2), 505–526. doi:10.1016/j.jrmge.2021.10.006

Lindquist, E. S. (1994). *The strength and deformation properties of melange*. Berkeley: University of California.

Liu, H. N., Zhang, Y. F., and Liu, H. D. (2019). Experimental study on active failure modes of slurryshield-driven tunnel faces in sand. *Chin. J. Rock Mech. Eng.*, 572–581. *March 2019)*.

Medley, E., and Goodman, R. E. (1994). Estimating the block volumetric proportions of melanges and similar block-in-matrix rocks (bimrocks). OnePetro. *1st North American Rock Mechanics Symposium*.

Medley, E. W., and SanzRehermann, P. F. (2004). Characterization of bimrocks (rock/soil mixtures) with application to slope stability problems. *Proc. EUROCK*.

Mollon, G., and Zhao, J. (2012). Fourier-Voronoi-based generation of realistic samples for discrete modelling of granular materials. *Granul. matter* 14 (5), 621–638. doi:10.1007/s10035-012-0356-x

Napoli, M. L., Barbero, M., Ravera, E., and Scavia, C. (2018a). A stochastic approach to slope stability analysis in bimrocks. *Int. J. Rock Mech. Min. Sci.* 101, 41–49. doi:10.1016/j.ijrmms.2017.11.009

Napoli, M. L., Barbero, M., and Scavia, C. (2018b). Analyzing slope stability in bimrocks by means of a stochastic approach. *ISRM, OnePetro*.

Napoli, M. L., Barbero, M., and Scavia, C. (2021). Tunneling in heterogeneous rock masses with a block-in-matrix fabric. *Int. J. Rock Mech. Min. Sci.* 138, 104655. doi:10.1016/j.ijrmms.2021.104655

Qiao, J. L., Zhang, Y. T., and Gao, J. (2010). Application of strength reduction method to stability analysis of shield tunnel face. *J. Tianjin Univ.* 43 (1), 14–20.

Shiau, J., and Asadi, F. (2020). Stability analysis of twin circular tunnels using shear strength reduction method. *Geotech. Lett.* 10 (2), 311–319. doi:10.1680/jgele.19.00003

Ukritchon, B., and Keawsawasvong, S. (2019b). Design equations of uplift capacity of circular piles in sands. *Appl. Ocean Res.* 90, 101844. doi:10.1016/j.apor.2019.06.001

Ukritchon, B., and Keawsawasvong, S. (2019a). Lower bound solutions for undrained face stability of plane strain tunnel headings in anisotropic and non-homogeneous clays. *Comput. Geotechnics* 112, 204–217. doi:10.1016/j.compgeo.2019.04.018

Ukritchon, B., and Keawsawasvong, S. (2017). Three-dimensional undrained tunnel face stability in clay with a linearly increasing shear strength with depth. *Comput. geotechnics* 88, 146–151. doi:10.1016/j.compgeo.2017.03.013

Ukritchon, B., Yoang, S., and Keawsawasvong, S. (2019). Three-dimensional stability analysis of the collapse pressure on flexible pavements over rectangular trapdoors. *Transp. Geotech.* 21, 100277. doi:10.1016/j.trgeo.2019.100277

Wang, Y., Zhao, M., Li, S., and Wang, J. G. (2005). Stochastic structural model of rock and soil aggregates by continuum-based discrete element method. *Sci. China Ser. E Eng. Mater. Sci.* 48, 95–106.

Xia, C., Xu, C., and Zhao, X. (2012). Study of the strength reduction DDA method and its application to mountain tunnel. *Int. J. Comput. Methods* 9 (03), 1250041. doi:10.1142/s0219876212500417

Xing, C., and Jianlin, L. I. (2010). The strength reduction method based on ADINA, ANSYS and FLAC. *Hydrogeology Eng. Geol.* 37 (3), 69–73.

Xu, W. J., Zhang, H. Y., and Xu, Q. (2014). Numerical simulations of direct shear test with soil-rock mixture using discrete element method. *Chin. J. Comput. Mech.* 31 (2), 228–234.

Xue, Y., Huang, H., and Griffiths, D. V. (2012). Specimen reconstitution and uniaxial compressive strength testing of rock-soil mixtures. *Adv. Ground Technol. Geo-Information* 289.

Yang, X., and Huang, F. (2009). Stability analysis of shallow tunnels subjected to seepage with strength reduction theory. *J. Central South Univ. Technol.* 16 (6), 1001–1005. doi:10.1007/s11771-009-0166-4

Zhang, C., Han, K., and Zhang, D. (2015). Face stability analysis of shallow circular tunnels in cohesive–frictional soils. *Tunn. Undergr. Space Technol.* 50, 345–357. doi:10.1016/j.tust.2015.08.007

Zhang, L. M., Zheng, Y. R., and Wang, Z. Q. (2007). Application of strength reduction finite element method to road tunnels. *Yantu Lixue (Rock Soil Mech.* 28 (1), 97–101.

Zhang, S., Zeng, Y. W., and Xia, L. (2016). Numerical study on the influence of rock mass content on the stability of soil rock mixture slope. *J. Yangtze River Sci. Res. Inst.* 33 (5), 83–87.

Zhang, Y., Chen, G., Wang, Z., and Liu, D. (2023). Fracture evolution analysis of rock bridges in hard rock with nonparallel joints in true triaxial stress states. *Rock Mech. Rock Eng.* 56, 997–1023. doi:10.1007/s00603-022-03117-x

Zhang, Y. X., Hu, J. Y., and He, Q. Y. (2006). On rational clear spacing of tunnel with small clear spacing based on strength reduction technique. *Hydrogeology Eng. Geol.* (3), 64–67.

Zheng, Y. R., Qiu, C. Y., and Zhang, H. (2008). Exploration of stability analysis methods for surrounding rocks of soil tunnel. *Chin. J. Rock Mech. Eng.* 27 (10), 1968–1980.

Zheng, Y. (2011). The application of FEM limit analysis in tunnel engineering. *J. Chongqing Jiaot. Univ. Nat. Sci.* 30 (S2), 1127.